Journal of Materiomics 7 (2021) 1061–1073

Contents lists available at ScienceDirect

Journal of Materiomics

journal homepage: www.journals.elsevier.com/journal-of-materiomics/

A new series of environment-friendly reddish inorganic pigments based on $AFeO_3$ (A = Ln, Y) with high NIR solar reflectance

Maria Fortuño-Morte, Pablo Serna-Gallén, Héctor Beltrán-Mir*, Eloísa Cordoncillo**

Departamento de Química Inorgánica y Orgánica, Universitat Jaume I, Av. Sos Baynat s/n, 12071, Castelló de la Plana, Spain

ARTICLE INFO

Article history:
Received 2 December 2020
Received in revised form
21 January 2021
Accepted 1 February 2021
Available online 11 February 2021

Keywords:
High NIR reflectance
Cool pigment
Reddish pigment
Environment-friendly
Coprecipitation

ABSTRACT

Environment-friendly pigments based on $AFeO_3$ (A = La, Pr, Nd, Sm, Gd, Tb, Y or Yb) with high near-infrared (NIR) reflectance were synthesised by a coprecipitation method at 1200 °C. The Rietveld refinement analysis showed single-phase orthorhombic perovskite for all compositions. All pigments, which showed reddish hues, offered good colour stability after mixing these pigments in powder form with siloxane transparent paint and two different glazes. The powder–paint mixtures produced with $GdFeO_3$, $TbFeO_3$ and $YFeO_3$ pigments have the highest NIR solar reflectance, reaching values of R = 50%. The temperature shielding studies conducted using $TbFeO_3$ pigment–paint mixture for a roof coating yielded a reduction of 3.2 °C in comparison to a commercial pigment. Moreover, the glazes that were pigmented using $GdFeO_3$, $TbFeO_3$ and $YFeO_3$ compositions also presented the most intense reddish colours. A study of the thermal and chemical stability of the pigment with the highest NIR solar reflectance showed good stability in both cases. The reddish pigments that were prepared can therefore be good candidates for use in different applications such as cool pigments or pigments for ceramic glazes at high temperatures.

1. Introduction

Over the last century, the average temperature of the Earth has increased by 0.8 °C [1]. Although this may seem an almost insignificant amount, small changes in temperature cause enormous changes in the environment [2–4]. Furthermore, scientists think that the global temperature will continue to rise, mostly because of greenhouse gases produced by human activities [5,6].

As climate change leads to higher ambient temperatures, urban areas will be the most affected by harsher heat events. Solar energy is absorbed by buildings, leading to an increase in the surface temperature and, consequently, also in the ambient temperature. This in turn results in a rise in energy consumption, especially because of the use of air conditioning. However, its use can be reduced by controlling the temperature within the building with materials known as 'cool pigments'. Due to the high solar reflectance and infrared emission of these compounds, applying them as a coating on roofs and walls decreases the temperature of the building envelope [7,8]. Consequently, the use of these compounds as a roof coating can help people adapt to the impacts of climate change as well as lower the greenhouse gas emissions that cause climate change.

It is well known that white pigments such as Al_2O_3, ZnO and TiO_2 present high near-infrared (NIR) reflectance [9]. However, although there are coloured pigments with this optical property [10], many of them contain heavy metals like Sb, Cd, Co, Cr, Pb or Ni as chromophore ions, and they are based on mixed metal oxides such us chromium oxide green, cobalt aluminate blue, cobalt chromite blue, strontium chromate yellow, cadmium stannate, lead chromate or nickel titanate, which can be detrimental to human health [11]. In recent years, some studies have developed new environment-friendly pigments with high NIR reflectance [12,13]. For example, Huang et al. [12] synthesised Pr^{4+} and Tb^{4+} doped $La_2Ce_2O_7$ pigments with high NIR solar reflectance. The substitution of Ce^{4+} by Pr^{4+} and Tb^{4+} changes the colour of this pigment from light yellow to soft orange and then dark orange. In another study, Dolić et al. [13] prepared yellow pigments based on $BiVO_4$ that present NIR reflectance higher than 80%.

Because the present study focuses on reddish cool pigments, it is important to know that Pb_3O_4, CdS·CdSe and HgS are the common

* Corresponding author.
** Corresponding author.
E-mail addresses: fortunom@uji.es (M. Fortuño-Morte), pserna@uji.es (P. Serna-Gallén), mir@uji.es (H. Beltrán-Mir), cordonci@uji.es (E. Cordoncillo).
Peer review under responsibility of The Chinese Ceramic Society.

https://doi.org/10.1016/j.jmat.2021.02.002

classical red pigments [14], despite the fact they all include toxic metal elements (Pb, Cd and Hg). Other industrial reddish pigments currently in use include Al_2O_3:Cr^{3+} (corundum), $CaSnSiO_5$:Cr^{3+} (sphene), $ZnAl_2O_4$:Cr^{3+} and $MnAl_2O_4$:Cr^{3+} (spinel), which contain chromium as the chromophore ion. Fortunately, the developed countries have taken an active stand towards the approval of regulations limiting the use of heavy and toxic metals in order to protect human health and the environment. As a result, over the last few decades other elements like iron, yttrium or lanthanides have emerged as potential alternatives to the use of the above-mentioned toxic ions [15–17].

Nowadays, one of the non-toxic reddish pigments that is most widely used in the ceramic industry is the iron-doped zircon pigment (Fe–$ZrSiO_4$). Nevertheless, the final colour of this compound is very difficult to control because it depends heavily upon the morphology and size of the particles in the reagents [18–20]. Furthermore, not only is the formation mechanism of the pigment under debate but questions are also being raised about the oxidation state and the position of iron in the structure [21–23]. As a result, the development of new environment-friendly reddish pigments is ongoing, with special attention being paid to those with high NIR reflectance [24,25].

The presence of lanthanides in inorganic pigments is an important alternative to obtain environment-friendly cool colourants, due to their distinctive optical properties. The group led by Vishnu and Reddy [26,27] developed two different inorganic pigments based on praseodymium-doped Y_6MoO_{12} and $Y_2Ce_2O_7$, which exhibited colours ranging from yellow to brick-red and from brick-red to dark-brown, respectively. They also showed significant NIR solar reflectance when applied as a coating on roofing materials like asbestos cement sheet. As a result, these elements provide final materials with an additional value, namely high NIR reflectance, which can be crucial to reduce the temperature increases of buildings [15,28].

Among many inorganic structures where lanthanides are easily incorporated, perovskite-type oxides, in particular AFeO$_3$ perovskites, have been considered of the utmost importance due to their great variety of physical and chemical properties, which provide them with several extraordinary applications as catalytic materials [29], sensors [30] or pigments [31]. Perovskites have the general formula ABO_3, where A and B are cations of very different sizes, A (with a coordination number, CN, of 12) being larger than B (with a CN of 6). Unfortunately, in none of the applications mentioned above has the use of AFeO$_3$ compounds as pigments been given the attention it deserves.

Several studies have analysed the optical properties, in terms of colouration, of some compounds with the perovskite structure AFeO$_3$ (A = lanthanide ion) [32–38], but NIR reflectance has not been measured in any of them. Regarding this kind of measurements in similar perovskites, Yuan et al. [39] reported high NIR solar reflectance (R > 44.1%) of pigments based on lanthanum-doped $BiFeO_3$ applied as a coating on a concrete cement substrate, and considered them good candidates for applications as cool pigments. However, these pigments were prepared at low temperatures, 600 °C for 24 h, and therefore applications at higher temperatures will be not possible. For example, these pigments will not be stable in glazes for tiles, where the pigment–frit mixture is usually fired at temperatures above 1000 °C. On the other hand, Liu et al. [28] developed brown and yellow pigments based on the nominal composition, $LaFe_{1-x}Al_xO_3$ (x = 0, 0.1, 0.3, 0.5, 0.7), that exhibited high NIR solar reflectance of coatings (from 38.7% to 45.8%) and, consequently, could also be used as cool pigments. It is important to note that, to the best of our knowledge, this is the only work to have conducted an accurate study of the optical properties of AFeO$_3$ perovskites, where A = lanthanide ion.

Hence, in this paper, environment-friendly reddish pigments based on the general formula AFeO$_3$, where A = La, Pr, Nd, Sm, Gd, Tb, Y or Yb, are studied for use as cool pigments. In the present work, a simple synthesis process based on the coprecipitation method has been implemented that could easily be carried out in an industrial process. The different applications of these materials in paint and glaze were studied. Special emphasis should be placed on the capacity of these pigments to present high NIR and solar reflectance and a good reddish colouration.

2. Experimental section

2.1. Materials and methods

AFeO$_3$ (A = La, Pr, Nd, Sm, Gd, Tb, Y or Yb) powders were prepared by a coprecipitation method using $Fe(NO_3)_3{\cdot}9H_2O$ (98%, Sigma-Aldrich) and the corresponding lanthanide precursor, that is, $La(NO_3)_3{\cdot}6H_2O$ (99.99%, Sigma-Aldrich), $Pr(NO_3)_3{\cdot}6H_2O$ (99.9%, Sigma-Aldrich), $Nd(NO_3)_3{\cdot}6H_2O$ (99.9%, Strem Chemicals), $Sm(NO_3)_3{\cdot}6H_2O$ (99.9%, Sigma-Aldrich), $Gd(NO_3)_3{\cdot}6H_2O$ (99.9%, Strem Chemicals), $Tb(NO_3)_3{\cdot}6H_2O$ (99.9%, Strem Chemicals), $Y(NO_3)_3{\cdot}6H_2O$ (99.8%, Sigma-Aldrich) or $Yb(NO_3)_3{\cdot}5H_2O$ (99.9%, Strem Chemicals), as starting materials. Besides, absolute ethanol (99.9%, Scharlab) was used as a solvent and reagent-grade ammonia solution (32%, Scharlab) was used as a precipitation agent.

A general scheme of the method employed is shown in Fig. 1. Briefly, in order to obtain an AFeO$_3$ compound, the stoichiometric amounts of the corresponding precursors were dissolved in different ethanol solutions stirred for 3 h. Subsequently, they were mixed and stirred continuously for a further 21 h at room

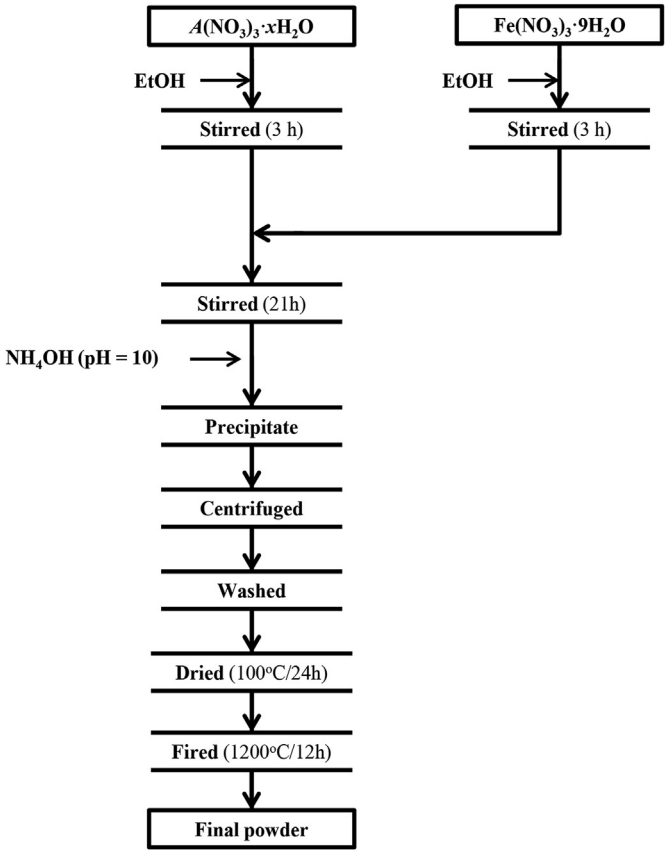

Fig. 1. Scheme for the synthesis procedure.

temperature. Afterwards, ammonia solution was added until pH ≈ 10 to obtain a precipitate. The mixture was centrifuged, washed with ethanol and dried, and the powder was then fired at a maximum temperature of 1200 °C for 12 h. The waste liquid that remains after the centrifugation process is a basic solution that contains ethanol/water and ammonium nitrate. Only this ammonium nitrate was detected by XRD after evaporation of the solvent. Finally, the fired pigments were sieved at 0.06 mm to evaluate their properties in three different commercial transparent mediums: a paint and two glazes.

To do so, double-fired white body ceramic tiles were coloured with homogeneous mixtures of siloxane transparent paint and pigment (10 wt% of the pigment) to evaluate the capacity of all the compounds as cool pigments.

Moreover, coloured pigments were mixed with two different frits (4 wt% of the pigment), whose compositions are shown in Table 1. In this study, two commercial frits with different compositions, currently used in the ceramic industry, were selected to study the interaction of the pigment–frit mixture. These mixtures were pressed into Ø 4 cm pellets, placed on a double-fired white body ceramic tile and then fired in an electric furnace at a maximum temperature of 1080 °C. The cycle, which is similar to that used in the ceramic industry for these glazes, involves five steps: ramping to 300 °C in 10 min, heating from 300 °C to glaze firing temperature in 17 min, holding at 1080 °C for 5 min, cooling to 600 °C in 20 min and, finally, cooling to room temperature in 15 min.

2.2. Characterisation techniques and instrumentation

X-ray diffraction (XRD) measurements for the powder were carried out on a Bruker-AXS D8 X-ray diffractometer with CuK_α radiation. All data were collected by step-scanning from $2\theta = 20$ to 90° at room temperature with a step size of 0.015° and a counting time of 0.4 s at each step. The experimental diffraction patterns of the powders were refined using the Rietveld method by means of FullProf software [40]. A Pseudo-Voight function was used to simulate the peak shape and a sixth-degree polynomial function for the background.

Microstructure characterisation and semi-quantitative chemical analysis of final powders were performed using a JEOL 7001F field emission scanning electron microscope (FE-SEM) equipped with an energy dispersive X-ray spectrometer (EDX), and an acceleration voltage of 15 kV. A semi-quantitative analysis was performed from the EDX analyses, taking an average of ten measurements in different particles. Samples for microstructure and microanalysis determinations were deposited in an aluminium holder and sputtered with platinum.

Raman spectra of the different compositions were recorded in the frequency range of 90–700 cm^{-1}, at room temperature, using a modular Raman system from WITec GmbH, based on an automatic vertical confocal microscope, model alpha300 apyron, with an EMCCD ultra-high efficiency detector refrigerated at −60 °C and equipped with a 532 nm laser coupled to the microscope.

Table 1
Compositions of frit A and frit B.

Frit	Composition (wt%)[a]						
	SiO_2	Al_2O_3	RO[b]	R_2O[b]	ZnO	PbO	ZrO_2
A	62.3	10.2	5.9	9.3	3.1	9.1	0.1
B	61.6	10.4	13.8	8.4	3.4	2.2	0.2

[a] The percentages do not represent quantitative analyses.
[b] R = alkali or alkaline earth metals.

The optical properties of the powdered pigments and pigmented paints were measured using a UV–Vis–NIR Jasco V670 spectrophotometer, which gives information about the absorbance in arbitrary units (a.u.) and the reflectance as a percentage, R (%). The Kubelka-Munk transformation model was also used. The reflection spectra were performed in the 300–2500 nm range with a 1 nm interval. The NIR solar reflectance (R_{NIR}) of each compound was obtained by equation (1), where $r(\lambda)$ is the spectral reflectance ($W \cdot m^{-2}$) measured from UV–Vis–NIR spectroscopy and $i(\lambda)$ is the standard solar irradiation ($W \cdot m^{-2} \cdot nm^{-1}$) obtained from ASTM standard G173-03 [41].

$$R_{NIR} = \frac{\int_{750}^{2500} r(\lambda) \cdot i(\lambda)\, d\lambda}{\int_{750}^{2500} i(\lambda)\, d\lambda} \quad (1)$$

CIE$L^*a^*b^*$ and CIE$L^*C^*H^\circ$ colour parameters of both the prepared pigments and their applications were obtained with a Konica Minolta CM-2300d Portable Spectrophotometer with a beam diameter of 8 mm and using a standard illuminant D65 to differentiate the pigment in terms of colour. In this method, L^* is a measure of lightness and takes values from 0 = black to 100 = white, a^* is the green (<0) to red (>0) axis, and b^* is the blue (<0) to yellow (>0) axis. The hue angle (H°) describes the relative amounts of redness and yellowness and can take values between 0° to 360°, the angle starting from magenta at 0° towards yellow at 90° and green and blue are positioned at 180° and 270°, respectively. Chroma (C^*) represents saturation of the colour. Both H° and C^* parameters are related by a^* and b^* parameters according to equations (2) and (3):

$$H^o = \arctan\left(\frac{b^*}{a^*}\right) \quad (2)$$

$$C^* = \sqrt{a^{*2} + b^{*2}} \quad (3)$$

The thermal stability of the pigments was studied by simultaneous thermogravimetry and differential scanning calorimetry (TG-DSC) on a Mettler Toledo analyser (model TGA/DSC3) in the temperature range of 50–1200 °C, under an air atmosphere, and at a heating rate of 10 °C/min.

The chemical stability of the pigments was evaluated using acid/alkali solutions and water. A small amount of the pigment with the best colour and reflectance was dispersed with 5% acid HNO_3, 5% alkali NaOH, and H_2O for 30 min with continuous stirring. The pigment powder was then filtered, washed with deionised water and subsequently dried, and the weight was estimated. The CIE colour coordinates were evaluated and the colour difference (ΔE^*) was determined using equation (4):

$$\Delta E^* = \sqrt{(\Delta L^*)^2 + (\Delta a^*)^2 + (\Delta b^*)^2} \quad (4)$$

where ΔL^*, Δa^* and Δb^* are the changes in L^*, a^* and b^*, respectively.

3. Results and discussion

Fig. 2 shows the XRD patterns and the Rietveld refinements with the χ^2 value for the fits of the final powders for each composition fired at 1200 °C. The χ^2 value is one of the most commonly used statistical parameters in Rietveld refinements that gives a clear idea about the goodness of fit. The χ^2 parameter is defined as the

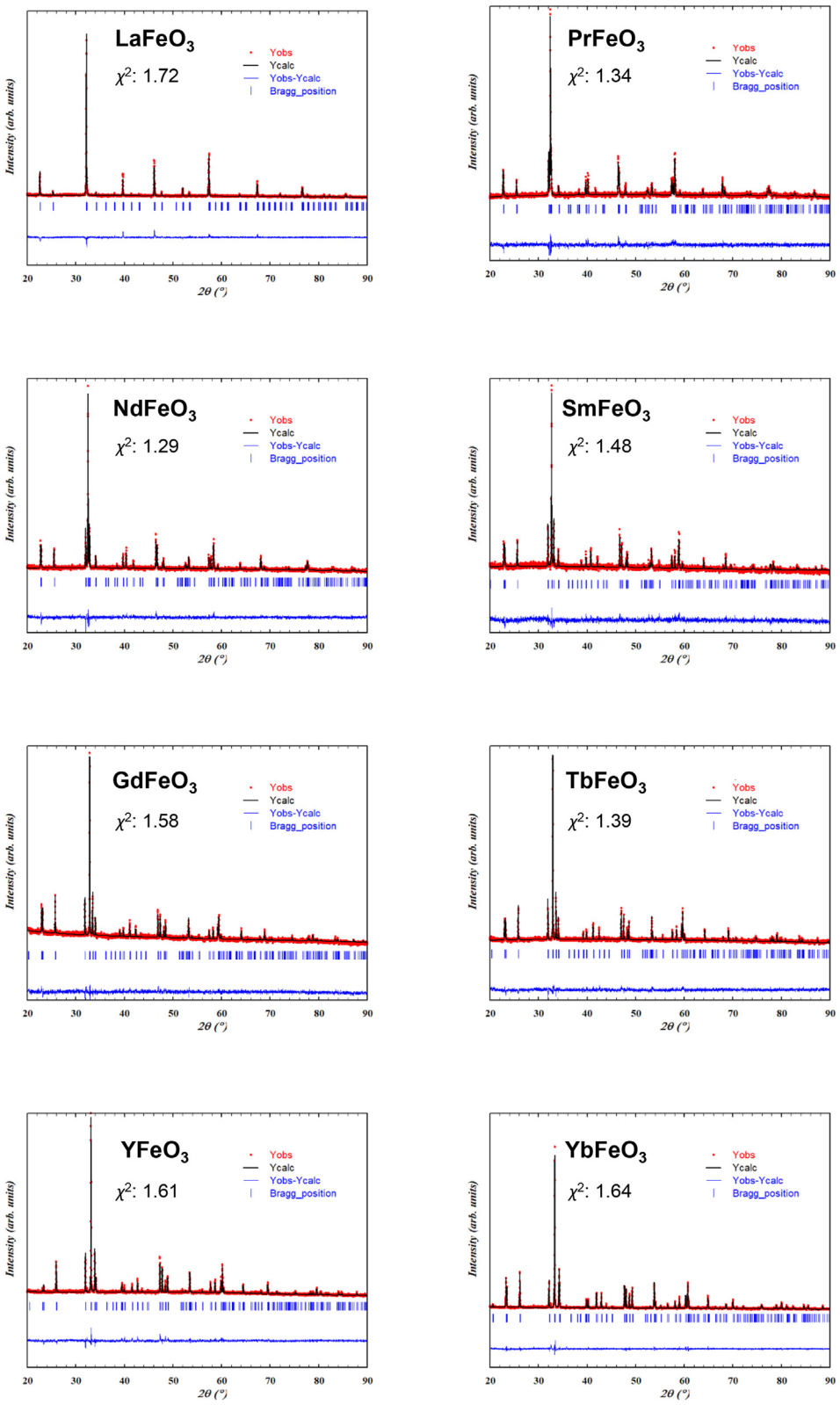

Fig. 2. Rietveld refinements of the $AFeO_3$ orthoferrites (A = La, Pr, Nd, Sm, Gd, Tb, Y or Yb).

squared ratio between the weighted-profile R-factor (R_{wp}) and the expected R-factor (R_{exp}), i.e. between the R-factor from the experimental refinement and the R-factor expected from counting statistics. For a good refinement, R_{wp} should be similar to the R_{exp} value. Consequently, χ^2 should ideally be close to unity (commonly in the range 1–2) because this parameter can be defined as:

$$\chi^2 = \left(\frac{R_{wp}}{R_{exp}}\right)^2 \quad (5)$$

The results showed that the refinements were correct and the orthorhombic perovskite phase with the *Pbnm* space group was observed in all samples without any secondary phases. The numbers of theoretical patterns used to identify the phase in each $AFeO_3$ composition were: $LaFeO_3$ [JCPDS-ICDD 74–2203], $PrFeO_3$ [JCPDS-ICDD 74–1472], $NdFeO_3$ [JCPDS-ICDD 74–1473], $SmFeO_3$ [JCPDS-ICDD 74–1474], $GdFeO_3$ [JCPDS-ICDD 47–67], $TbFeO_3$ [JCPDS-ICDD 47–68], $YFeO_3$ [JCPDS-ICDD 86–171] and $YbFeO_3$ [JCPDS-ICDD 74–1482]. The refined unit cell parameters for the different $AFeO_3$ orthoferrites are presented in Table 2.

This orthorhombic structure can be derived from the ideal cubic perovskite structure by rotations (tilts) of its FeO_6 octahedra and the tilt angles can be tuned by the size of the *A* lanthanide [42] (Fig. 3). It should also be taken into consideration that *Pbnm* and *Pnma* are structurally equivalent space groups differing in the choice of the unique axis; the transformation between *Pbnm* and *Pnma* corresponds to a cyclic perturbation of the axis [43]. For the purpose of this study, *Pbnm* was chosen.

Moreover, the stability and the distortion of the perovskite structure due to the size variation of the *A* site ion are indicated by the Goldschmidt tolerance factor, which can be defined with equation (6):

$$t = \frac{r_A + r_O}{\sqrt{2}(r_B + r_O)} \quad (6)$$

For an ideal cubic structure, *t* is close to 1, otherwise it has a distorted structure, for example, orthorhombic, rhombohedral or tetragonal [44]. The tolerance factors of the $AFeO_3$ orthoferrites were calculated taking into account the corresponding ionic radii of the different lanthanides with a CN = 12 [45] (Table 2). In all cases, the tolerance factor was lower than unity, meaning that the A^{3+} ions were smaller than the dodecahedral interstices. Consequently, the FeO_6 octahedra, Fig. 3b, tilt and rotate leading to closer packing with an orthorhombic structure *Pbnm* (*Pnma*) [46]. As the ionic radius of A^{3+} increases, the tolerance factor also increases. Thus, the lower the ionic radius of the lanthanide ion is, the closer the perovskite will be to having an orthorhombic structure.

Octahedral distortion plays a key role in the properties of the orthoferrite, especially considering the polarisation of the structure. The octahedral distortion can be estimated by calculating the octahedral tilt angle [47] in accordance with equation (7):

$$\phi = \frac{180^\circ - \theta}{2} \quad (7)$$

where θ is the bond angle of Fe–O–Fe along the *c* direction, shown in Fig. 3c, and is obtained from the crystal structure representation using the experimental atomic data obtained in the Rietveld refinements.

There is a clear tendency in the $AFeO_3$ sequence: the octahedral tilt angle becomes larger as the ionic radius increases, except for a small difference in $YbFeO_3$ (see Table 2). Therefore, these changes in the polarisation of the perovskite may be closely related to the different colours of the powders that were prepared, since the overlap between the *d* orbitals of Fe^{3+} and the *p* orbitals of O^{2-} is affected by octahedral tilting [46]. Furthermore, these different octahedral distortions in the compounds studied could also affect absorption in the NIR, that is, the energy of the vibration modes.

The microstructures obtained by SEM for the orthoferrites fired at 1200 °C for 12 h are shown in Fig. 4. The morphology of the particles of the ceramic powders was similar. However, the particle size was quite different for each compound. Whereas $PrFeO_3$, $SmFeO_3$ and $YbFeO_3$ presented the highest particle size (around 1 μm), the other samples had a smaller particle size, which was lower for $LaFeO_3$, $TbFeO_3$ and $YFeO_3$. In addition, on studying different sample zones, EDX reveals that there is no evidence of secondary phases in any of the samples and a homogeneous distribution of the elements in the samples was observed. The EDX analyses for all compositions are listed in Table S1 of the Supplementary Information (SI), and an EDX spectrum with the region where the microanalysis was performed for the $TbFeO_3$ composition is shown as an example in Fig. S1 of the SI. In fact all the compounds presented similar atomic proportions of lanthanide, iron and oxygen, corresponding to the stoichiometric perovskite composition $AFeO_3$.

To further confirm $AFeO_3$ structures, Raman spectra were obtained at room temperature from all the final powders in the range 90–700 cm^{-1}, as shown in Fig. 5a. As indicated above, $AFeO_3$ compounds present an orthorhombic structure. According to group theory, orthoferrites with the *Pbnm* space group have 24 Raman-active modes, which can be represented with Mulliken symbols as $\Gamma = 7\,A_g \oplus 7\,B_{1g} \oplus 5\,B_{2g} \oplus 5\,B_{3g}$ [43].

For orthorhombic perovskite with the general formula $AFeO_3$, Raman modes involve vibrations of *A* and oxygen ions. Fe^{3+} ions are in centres of inversion in the *Pbnm* structure. Therefore, these ions do not present Raman-active vibrations. According to the literature [48,49], the wavenumber modes below 200 cm^{-1} are mainly attributed to displacements of lanthanide ions in position *A*, because of vibrations of *A* and O, specifically *A*–O stretching vibrations. Raman peaks in the region between 200 cm^{-1} and 350 cm^{-1} are related to FeO_6 octahedral tiling. Besides, active bands from 350 cm^{-1} to 500 cm^{-1} correspond to out-of-phase oxygen bending motions, specifically, oxygen octahedral bending vibrations. Finally, symmetric Fe–O stretching vibrations appear above 500 cm^{-1}.

The sums of the Lorentzian functions were used to carry out the spectra deconvolution and thus determine the position of the different modes. The deconvolution of the $TbFeO_3$ spectrum is shown in Fig. 5b as an example. Additionally, the peak positions of each compound under study are listed in Table S2 of the SI, and are

Table 2
Ionic radii of the A^{3+} lanthanides (with a CN = 12), tolerance factor *t*, refined unit cell parameters, and tilt angle ϕ of the $AFeO_3$ orthoferrites (*A* = La, Pr, Nd, Sm, Gd, Tb, Y or Yb).

Powder	A^{3+} (Å)	*t*	*a* (Å)	*b* (Å)	*c* (Å)	Volume (Å^3)	ϕ (°)
$LaFeO_3$	1.36	0.954	5.5545(2)	5.5624(3)	7.8518(3)	242.59(3)	9.4
$PrFeO_3$	1.32	0.941	5.4843(2)	5.5732(2)	7.7875(2)	238.02(2)	13.0
$NdFeO_3$	1.31	0.937	5.4531(2)	5.5844(2)	7.7642(3)	236.44(3)	14.0
$SmFeO_3$	1.28	0.927	5.3986(2)	5.5947(2)	7.7070(3)	232.78(3)	15.6
$GdFeO_3$	1.27	0.923	5.3490(2)	5.6078(2)	7.6677(3)	230.00(3)	18.6
$TbFeO_3$	1.25	0.916	5.3288(1)	5.5985(1)	7.6424(2)	228.00(1)	19.6
$YFeO_3$	1.23	0.909	5.2816(1)	5.5915(1)	7.6041(2)	224.57(1)	20.9
$YbFeO_3$	1.20	0.899	5.2315(2)	5.5567(2)	7.5697(1)	220.05(2)	19.3

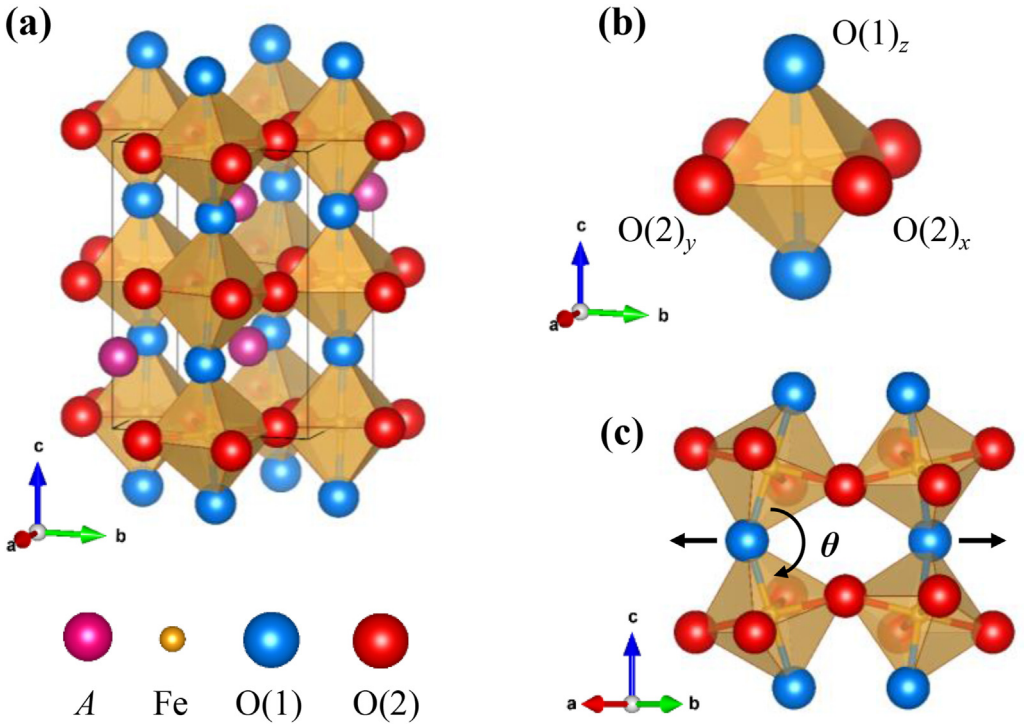

Fig. 3. a) General representation of the crystal structure of the $AFeO_3$ orthoferrites; b) Detail of an FeO_6 octahedron depicting the different oxygen atoms and their labels; c) Projection of the octahedra showing the displacement caused by the octahedral tilt (black arrows).

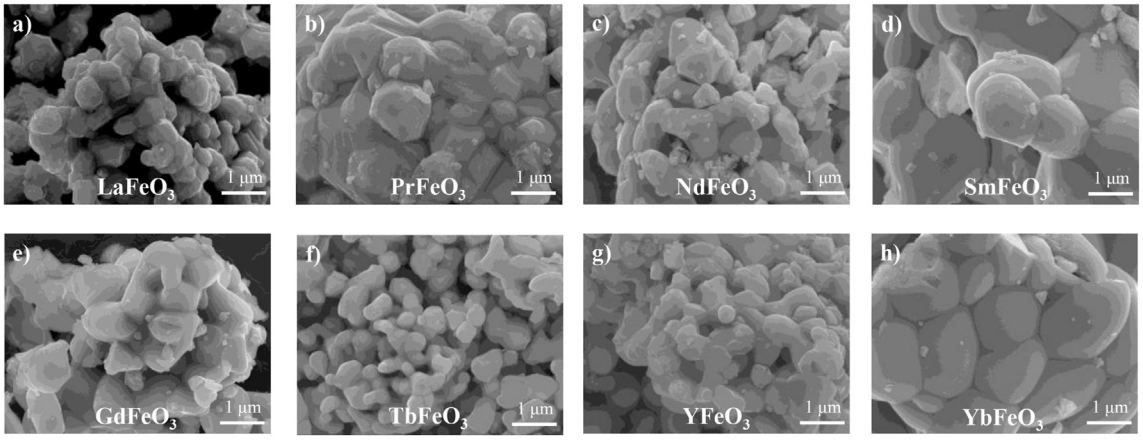

Fig. 4. Micrographs of the powders fired at 1200 °C: a) $LaFeO_3$, b) $PrFeO_3$, c) $NdFeO_3$, d) $SmFeO_3$, e) $GdFeO_3$, f) $TbFeO_3$, g) $YFeO_3$, and h) $YbFeO_3$.

consistent with previously reported literature [42,48,50]. Not all the predicted modes were identified because, presumably, some of them are either masked by band overlap or their intensity is below the detection limit. The differences between the Raman spectra of the compounds are due to the different distortions caused by each lanthanide. Nonetheless, the Raman results supported those obtained by XRD Rietveld refinement analysis.

The optical properties of the orthoferrites that were synthesised were studied using the UV–Vis reflectance and absorbance spectra of the fired powders in the 300–750 nm range shown in Fig. 6. For these compounds, the $O_{2p} \rightarrow Fe_{3d}$ charge transfer transitions and the 3*d*-3*d* transitions of Fe^{3+} are observed in these spectra. As can be seen in the UV–Vis reflectance spectra (Fig. 6a), an intense band is exhibited at ~600 nm in all cases, thus confirming the reddish pigmentation. With respect to the absorbance spectra (Fig. 6b), all the samples present a similar spectrum, dominated by a broad and intense band that appears at wavelengths between 350 and 550 nm. As shown in Fig. S2 of the SI, where the absorbance spectrum deconvolution of $TbFeO_3$ is presented as an example, a band was obtained around 350 nm, which corresponds to the $O_{2p} \rightarrow Fe_{3d}$ charge transfer transitions [51]. Moreover, in $AFeO_3$ compounds, 3*d*-3*d* transitions of Fe^{3+} ions generate the other four broad bands that can be found by deconvolution in the range that was studied. One of them was found at around 400 nm ($^6A_1 \rightarrow {}^4E$, $^4T_2$ transition), another at about 460 nm ($^6A_1 \rightarrow {}^4E$, ^4A transition), the third appeared at approximately 540 nm ($^6A_1 \rightarrow {}^4T_2$ transition) and the last one was observed at 700 nm ($^6A_1 \rightarrow {}^4T_1$ transition) [51].

The absorptions of trivalent lanthanide ions are very weak because the 4*f*-4*f* transitions are forbidden by Laporte's parity selection rule. In these cases, unlike the wide bands generated by

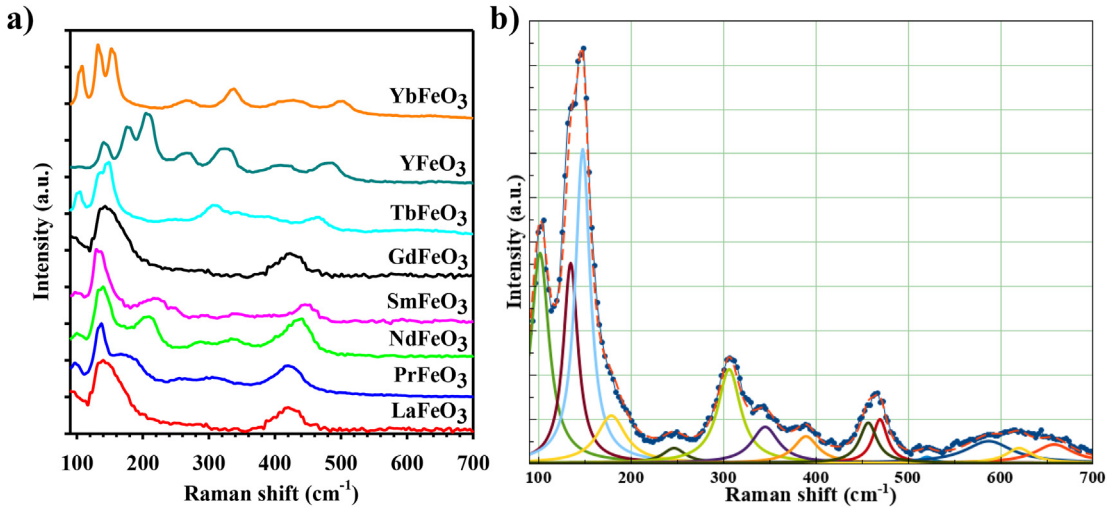

Fig. 5. a) Raman spectra of $AFeO_3$ (A = La, Pr, Nd, Sm, Gd, Tb, Y or Yb) samples; b) Raman spectrum deconvolution of $TbFeO_3$.

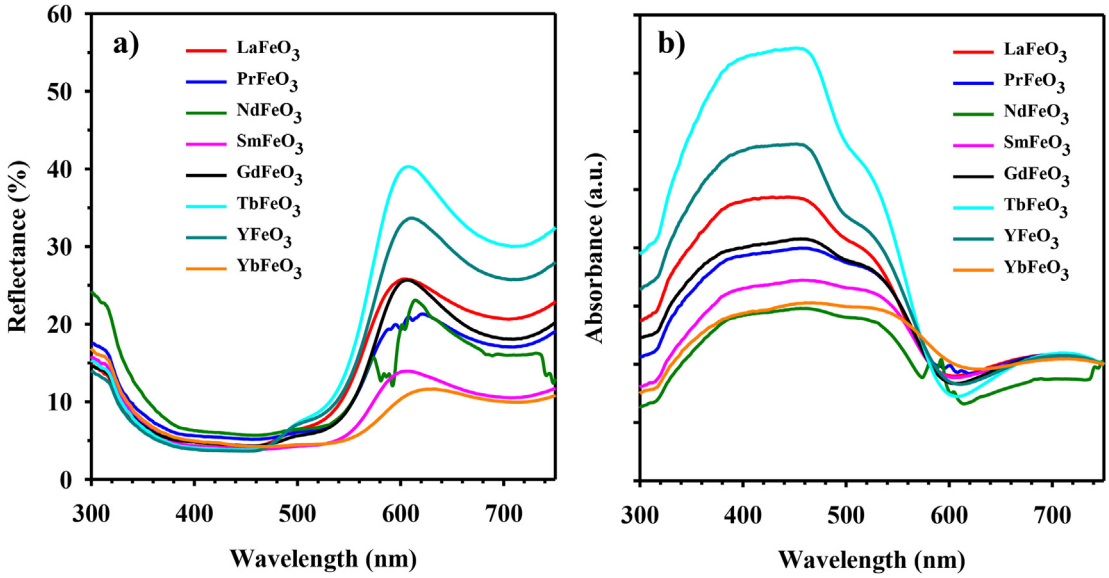

Fig. 6. a) UV–Vis reflectance spectra of $AFeO_3$ (A = La, Pr, Nd, Sm, Gd, Tb, Y or Yb) powders; b) UV–Vis absorption spectra of $AFeO_3$ (A = La, Pr, Nd, Sm, Gd, Tb, Y or Yb) powders.

transition metals, sharp absorption lines are originated and each group of lines corresponds to transitions between two $^{2S+1}L_J$ multiplets of the $4f^n$ configuration. As a consequence, it is difficult to see the trivalent lanthanide ion transitions that are found from 300 nm to 580 nm [52].

A better idea of the colour of the final powders is obtained from the band gap. The band gap energy of each of the synthesised pigments was determined using the Kubelka-Munk transformed reflectance spectra (Fig. 7) and similar values between 1.94 and 2.13 eV were found. Taking into account the statistical error that can occur in the measurements, the band gap results for the final powders were practically constant. Consequently, these energy values corresponded to the blue-green region of the visible spectrum and a complementary reddish colour was observed [53].

In order to gain a deeper knowledge of the orthorhombic perovskites prepared in this study, it is important to determine their NIR reflectance spectra. In this case, significant differences for each compound can be appreciated in Fig. 8; $GdFeO_3$, $TbFeO_3$ and $YFeO_3$ are the samples that exhibit the highest NIR reflectance, with values around 75%. The NIR solar reflectance values of the pigments are presented in Table 3. The best NIR solar reflectance results are also obtained for $GdFeO_3$, $TbFeO_3$ and $YFeO_3$ powders with 43%, 48% and 47%, respectively. This fact makes them interesting candidates for use as cool pigments with a significant energy saving performance.

Taking into account all the results, a relation can be seen between the particle size and the solar NIR reflectance. Powders that present the highest particle size, around 1 μm, ($PrFeO_3$, $SmFeO_3$ and $YbFeO_3$) have the lowest NIR reflectance, and also present low values for the band gap energy. Moreover, the absorbance generally decreases as the particle size increases. The higher NIR reflectance obtained for the $GdFeO_3$, $TbFeO_3$ and $YFeO_3$ powders could therefore be attributed to the lower particle size of these pigments.

The chromatic properties of the $AFeO_3$ pigment samples, the colours of which are presented in Fig. 9, were evaluated by the CIE$L^*a^*b^*$ and CIE$L^*C^*H^\circ$ parameters listed in Table 3. Similar values of L^* were obtained for all the samples, ranging from 47.52 to 60.47. As regards the other colour coordinates, positive values of a^*

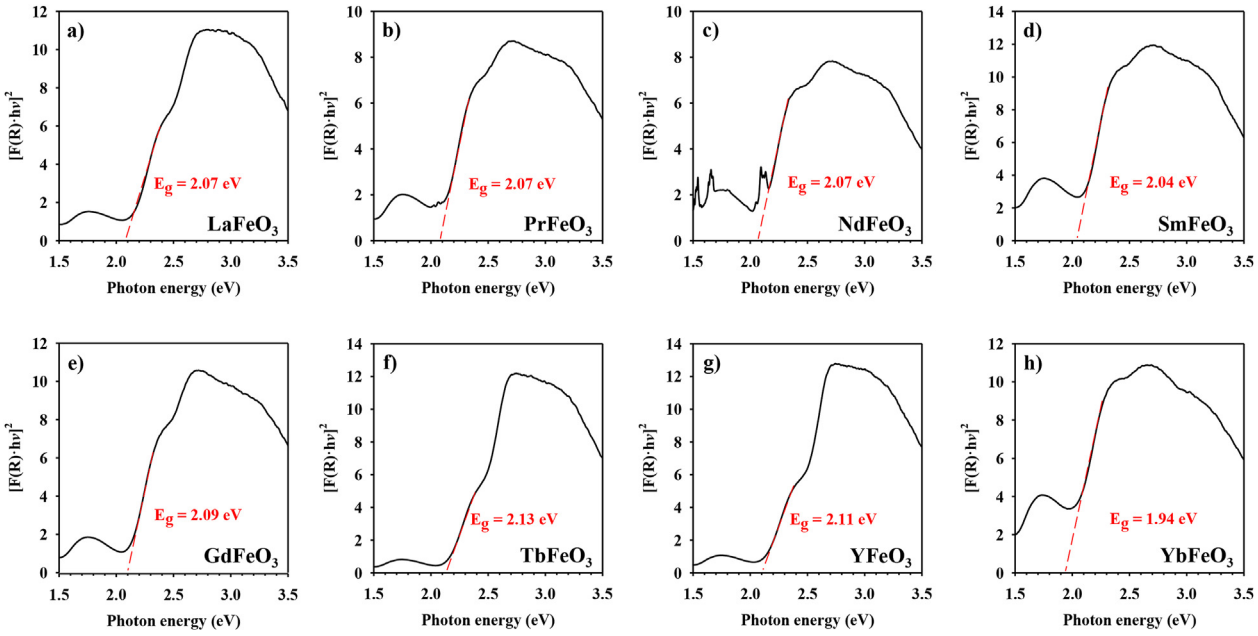

Fig. 7. Kubelka-Munk transformed reflectance spectra of the powders fired at 1200 °C: a) $LaFeO_3$, b) $PrFeO_3$, c) $NdFeO_3$, d) $SmFeO_3$, e) $GdFeO_3$, f) $TbFeO_3$, g) $YFeO_3$, and h) $YbFeO_3$.

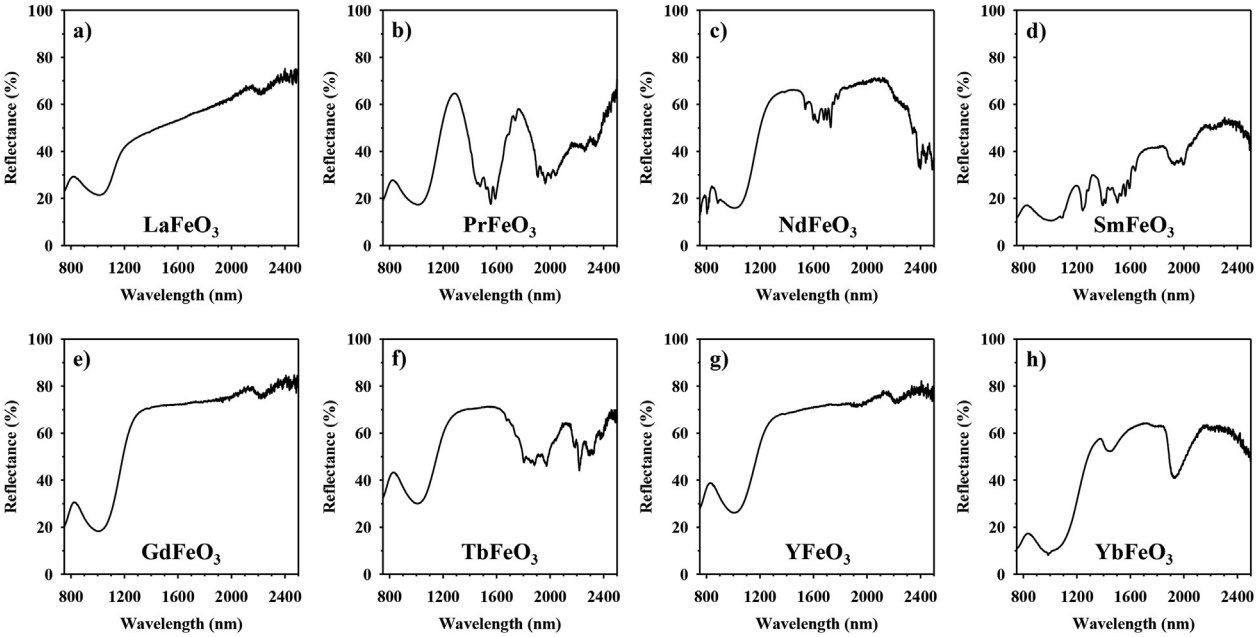

Fig. 8. NIR reflectance spectra of the powders fired at 1200 °C: a) $LaFeO_3$, b) $PrFeO_3$, c) $NdFeO_3$, d) $SmFeO_3$, e) $GdFeO_3$, f) $TbFeO_3$, g) $YFeO_3$, and h) $YbFeO_3$.

Table 3
Chromatic coordinates and NIR solar reflectance of the powder samples fired at 1200 °C for 12 h and pigments mixed with siloxane transparent paint.

Sample	Powder						Paint					
	L^*	a^*	b^*	C^*	H°	R_{NIR} (%)	L^*	a^*	b^*	C^*	H°	R_{NIR} (%)
$LaFeO_3$	55.48	16.83	26.27	44.32	61.97	37	48.10	19.97	36.12	41.17	61.10	43
$PrFeO_3$	52.37	16.02	19.18	35.91	54.19	33	44.66	19.95	28.72	34.91	55.29	37
$NdFeO_3$	50.43	14.36	14.34	21.99	45.84	36	45.98	20.24	26.13	33.23	52.34	44
$SmFeO_3$	51.06	13.70	14.76	18.73	46.86	21	43.29	18.38	24.54	31.00	53.38	31
$GdFeO_3$	54.99	19.14	23.64	43.45	55.41	43	47.12	23.71	34.61	42.12	55.74	47
$TbFeO_3$	60.47	21.94	32.22	40.26	56.01	48	52.75	25.66	45.17	52.04	60.45	50
$YFeO_3$	59.91	20.01	30.96	35.90	56.45	47	49.36	23.18	40.03	45.74	60.02	45
$YbFeO_3$	47.52	11.35	8.65	13.77	36.97	30	36.83	17.00	16.28	22.81	43.58	39

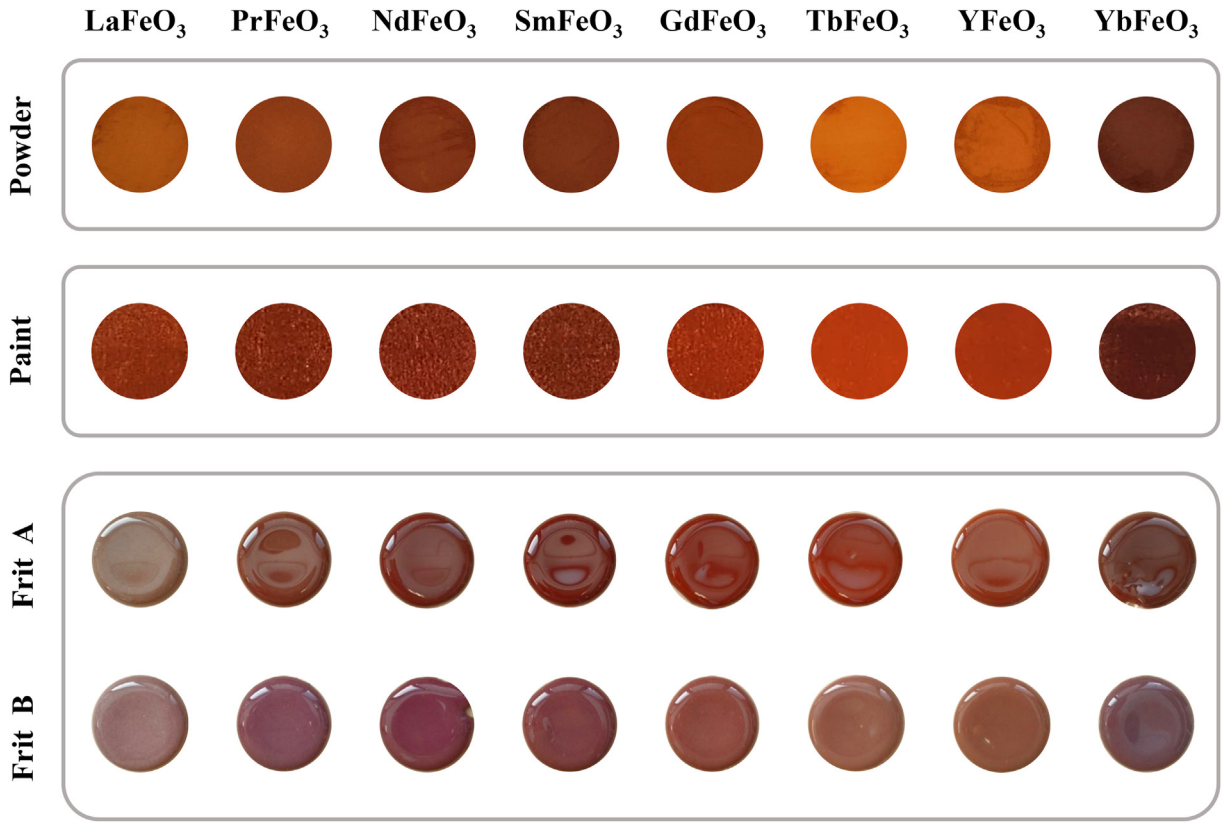

Fig. 9. Photographs of the powders, the pigment–siloxane paint mixtures and the pigments with glazes (frit A and frit B).

and b^* from 11.35 to 21.94 (red) and 8.65 to 32.22 (yellow) were observed, respectively. The range of C^* values was between 13.77 and 44.32, and with respect to the last parameter determined, H°, they ranged between 36.97° and 61.97° (magenta = 0° and yellow = 90°). All the powders prepared in this study presented a good reddish colouration, as can be appreciated in Table 3. Specifically, $GdFeO_3$, $TbFeO_3$ and $YFeO_3$ orthoferrites, which also presented the highest octahedral tilt angle (Table 2), had the highest values of a^* (red parameter). However, H° values were much lower for $NdFeO_3$, $SmFeO_3$ and $YbFeO_3$ and, consequently, these orthoferrites presented the reddest colouration.

Although it is important to know the factors that affect the final colour of the powders, it is also fundamental to study their applications in different materials. One of the most common implementations of inorganic pigments is to decorate ceramic tiles. However, these compounds can be used in other attractive applications as cool pigments when they present high NIR reflectance.

Evaluation of the colouring and thermal performance of the pigments in paint and glazes.

A pigment should be stable and exhibit an acceptable colourimetric performance when added (and thermally treated when needed) to different media such as paints or glazes.

Therefore, once the powders fired at 1200 °C had been characterised, their stability and colourimetric performance in a siloxane transparent paint and in two conventional glazes (firing temperature 1080 °C) were studied to examine their multifunctional applications. As shown in Fig. 9, all the powders presented good stability in these media, either maintaining or improving their colour performance.

The coloured paints thus prepared were applied on double-fired white body ceramic tiles. As shown in Fig. 9, the pigmented coating samples presented a homogeneous colour and a good reddish colouration similar to the final powders. CIE$L^*a^*b^*$ and CIE$L^*C^*H^\circ$ parameters were obtained in all of them and are listed in Table 3. Values of L^*, which ranged between 36.83 and 52.75, decreased in comparison to the powders. However, a^* and b^* had values from 17.00 to 25.66 (red) and 16.28 to 45.17 (yellow), respectively. An increase in these chromatic parameters with respect to the powders was found, and was more significant for b^*.

The saturation (C^*) and hue angle values, H°, of the coloured paints mainly increased with respect to the powders prepared in the study. Finally, $NdFeO_3$, $SmFeO_3$ and $YbFeO_3$ were the pigmented paints that presented the reddest colouration, as occurred with the powders.

The application of the powders incorporated into paint is the most appropriate presentation of these inorganic pigments to test the property of solar reflectance. The NIR reflectance spectra of the pigmented paints applied as a coating on ceramic tiles, which are shown in Fig. 10, were very similar to the NIR reflectance spectra of the powders. However, the pigmented coating possessed higher NIR reflectance values than the final powders. $GdFeO_3$, $TbFeO_3$ $YFeO_3$ and $YbFeO_3$, which are the samples that exhibited the highest NIR reflectance, presented reflectance values of around 80%. Moreover, the NIR solar reflectance values of the coatings, displayed in Table 3, were higher than the corresponding powdered pigments in all cases, except for $YFeO_3$, which had a similar NIR solar reflectance. Nonetheless, the highest NIR solar reflectance results were also obtained for $GdFeO_3$, $TbFeO_3$ and $YFeO_3$, with 47%, 50% and 45%, respectively. Moreover, five of the $AFeO_3$ pigment–paint mixes studied here, in particular compounds with A = La, Nd, Gd, Tb or Y, presented higher NIR solar reflectance values than reddish conventionally pigmented coatings of a similar colour, which have NIR solar reflectance values of around 42% [39]. Based on the NIR solar reflectance values obtained, $GdFeO_3$, $TbFeO_3$

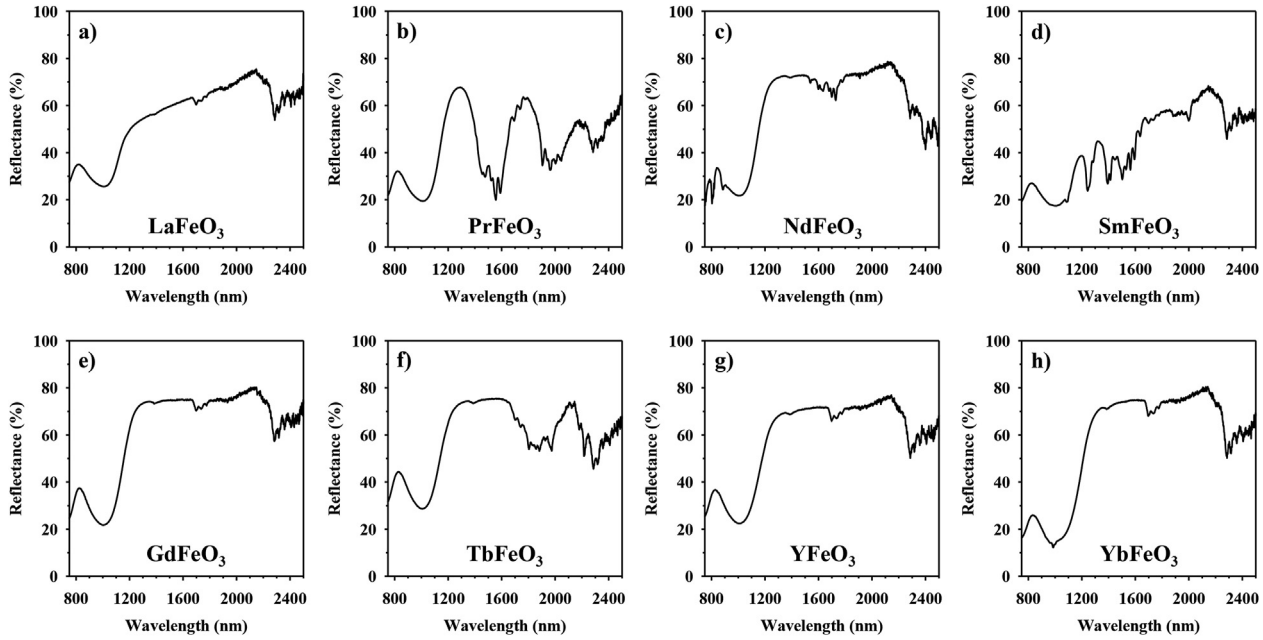

Fig. 10. NIR reflectance spectra of the pigment–siloxane paint mixtures fired at 1200 °C: a) $LaFeO_3$, b) $PrFeO_3$, c) $NdFeO_3$, d) $SmFeO_3$, e) $GdFeO_3$, f) $TbFeO_3$, g) $YFeO_3$, and h) $YbFeO_3$.

and $YFeO_3$ could be considered good cool pigments.

Consequently, to confirm the possible utility of the orthoferrites as cool pigments, a study was conducted with the powder–siloxane paint mixture that presented the highest NIR solar reflectance (sample of $TbFeO_3$). Thus, two foam buildings (5.5 cm × 5.5 cm × 7.5 cm; thickness of 0.7 cm) with different ceramic roof coatings consisting of paint mixed with the pigment –$TbFeO_3$ powder in one of them and a commercial reddish pigment based on Fe–$ZrSiO_4$ (Dry Colour Manufacturers' Association, DCMA 14-44-5) in the other– were exposed under an infrared lamp (Philips, 250 W). NIR reflectance of this commercial pigment is shown in Fig. S3 of the SI. In both cases the variation in temperature inside the structures was evaluated over time. A low temperature thermocouple was used to record the temperature at 5 min intervals and the temperatures obtained at the different times for each building are shown in Fig. 11. The inset in Fig. 11 shows the equipment used to test the temperature of the building with the coating of powder–paint mixtures. At all the times examined, the temperature of the paint with a commercial pigment was higher than the temperature of the $TbFeO_3$ pigmented paint. The temperature difference (ΔT) reached a maximum value of 3.2 °C at 60 min, where the temperature of the $TbFeO_3$ coating levelled out. As a result, the synthesised pigments could be used as cool roofing materials.

Regarding the application of pigments in glaze, Fig. 9 shows photographs of the powders after glazing at 1080 °C with two different frits, and their new chromatic coordinates are listed in Table 4. Although homogenous pigmentation was observed in all cases, differences in shading between frit A and frit B were obtained. In general, a small decrease in L^* values and similar results for a^* parameters were obtained for pigmented frits with respect to the final powders. Thus, the significant colour change was related to variations in b^* and, in keeping with equations (2) and (3), also in H° and C^* parameters. Despite this, regarding the colour of these pigments, good stability was observed in both cases when the pigments were mixed with two commercial frits and fired at 1080 °C.

In frit A, a decrease in b^*, C^* and H° was produced, in comparison to the powders. As a result, a better reddish colouration was obtained for colours of the final pigmented frit A. Samples with lower C^* values, $LaFeO_3$, $PrFeO_3$, $NdFeO_3$, $SmFeO_3$ and $YbFeO_3$, displayed a dark red colour. In contrast, the $GdFeO_3$, $TbFeO_3$ and $YFeO_3$ samples presented the highest a^* and C^* values, giving them more intense reddish colours.

Results for frit B showed b^* values of between −1.27 and 8.53. $NdFeO_3$ and $YbFeO_3$ orthoferrites presented negative b^* values ($b^* < 0$, blue colour). Based on C^* and H° values, frit B mixtures presented a lower intensity and a higher magenta tone ($H^\circ = 0$) than coloured frit A mixtures. Although there is a small variation in the colouration associated with a possible interaction of the pigment with the frits, the possible solid solution formed is very difficult to determine given the small amount of pigment used with respect to the frit (4%). However, XRD confirmed that the crystalline phase of the pigment remained after treatment of the pigment–frit mixture at 1080 °C. Fig. S4 of the SI shows the XRD of the pigment–frit A mixture after treatment at 1080 °C using the $YFeO_3$ pigment. In this XRD pattern, the main peaks of the perovskite were observed together with the typical amorphous halo of the majority vitreous matrix. Similar results were obtained for the other compositions. Therefore, although there is an interaction of the pigments with the frit, which modifies the crystalline environment of the chromophore element and therefore slightly alters the final colouration, the crystalline phase of the pigment remains after treatment.

3.1. Thermal and chemical stability studies of the pigments

$TbFeO_3$ was selected to evaluate the thermal and chemical stability of the synthesised pigments, because it was the compound that presented the highest NIR solar reflectance.

The thermal stability of $TbFeO_3$ was studied by thermogravimetric analysis in the temperature range from 50 °C to 1200 °C. Fig. S5 of the SI shows the TG-DSC curves for $TbFeO_3$ pigment. The results indicate that there is a negligible change in weight and phase transition of the pigment in this temperature range, which demonstrates that this pigment is thermally stable.

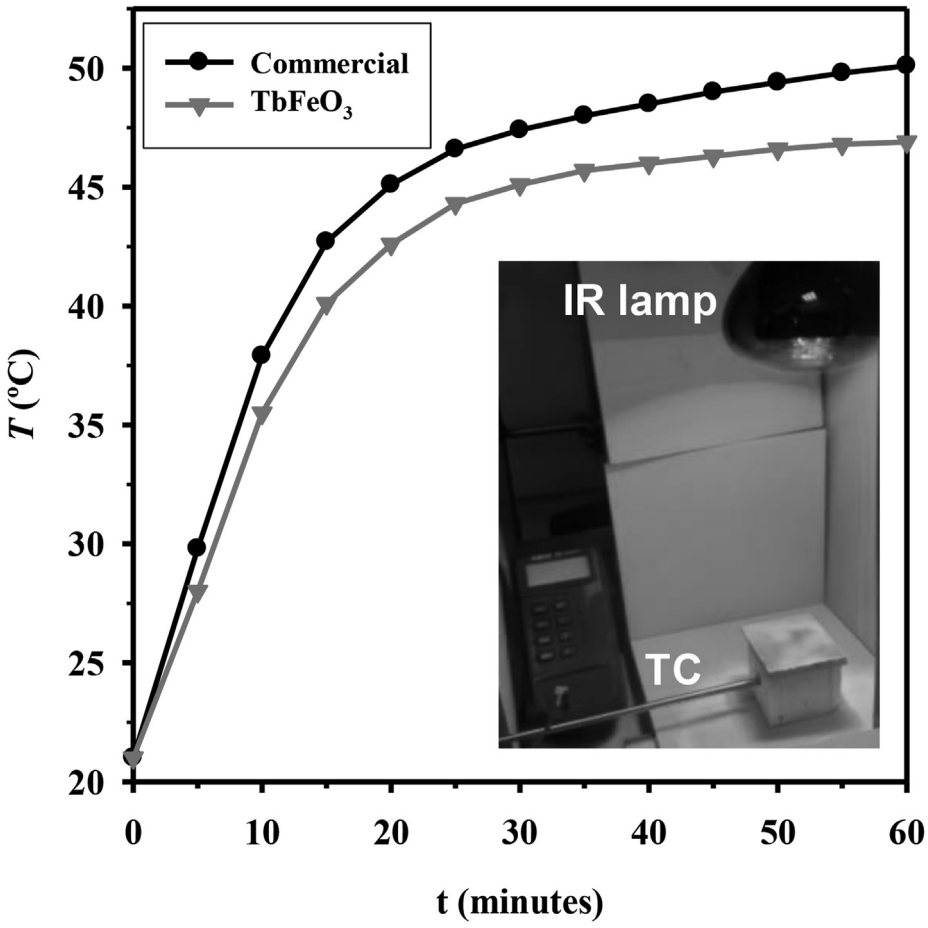

Fig. 11. The temperature inside the structures covered with $TbFeO_3$ powder and a commercial reddish pigment. Inset shows the equipment used to test the temperature of the building with the coating of powder–paint mixtures using a low temperature thermocouple (TC).Table 5. Final weight, chromatic coordinates and the total colour differences (ΔE^*) of the $TbFeO_3$ pigment after treatment in the different media.

Table 4
Chromatic coordinates of pigments mixed with glazes (frit A and frit B).

Sample	Frit A					Frit B				
	L^*	a^*	b^*	C^*	H°	L^*	a^*	b^*	C^*	H°
$LaFeO_3$	45.55	8.64	8.36	13.95	45.40	48.72	10.49	2.49	12.29	15.86
$PrFeO_3$	35.27	10.92	8.18	20.95	41.89	40.07	13.90	0.90	17.24	4.51
$NdFeO_3$	32.19	12.27	6.77	13.97	28.85	37.78	13.13	−1.25	13.33	354.21
$SmFeO_3$	31.18	13.21	7.43	15.14	29.37	38.56	13.02	1.28	13.08	5.52
$GdFeO_3$	32.30	17.42	11.55	27.23	35.78	41.64	14.77	6.17	3.93	358.17
$TbFeO_3$	33.84	20.97	16.65	25.83	37.84	44.68	14.39	7.60	16.28	27.94
$YFeO_3$	34.33	18.65	17.43	25.63	43.29	42.89	13.16	8.53	15.67	33.10
$YbFeO_3$	30.72	10.24	6.51	11.92	32.15	38.59	9.32	−1.27	9.46	352.56

To examine the chemical stability of $TbFeO_3$ powder, tests were carried out to determine the resistance of this compound to acid, alkali and water in 5% HNO_3 and 5% NaOH solutions and water. In all cases, 0.2500 g of $TbFeO_3$ powder was soaked with the different solutions for 30 min with constant stirring using a magnetic stirrer. The samples were then filtered, rinsed with water, dried and weighed again. The final weight, the chromatic coordinates and the total colour differences (ΔE^*) of the $TbFeO_3$ pigment after the treatment in the different media are listed in Table 5. A negligible weight loss was detected and small variations in the CIE$L^*a^*b^*$ parameters of the tested sample, and consequently low values of total colour differences (ΔE^*), were observed. The $TbFeO_3$ pigment that was synthesised was thus proved to be chemically stable in acid, alkali or water media.

Table 5
Final weight, chromatic coordinates and the total colour differences (ΔE^*) of the $TbFeO_3$ pigment after treatment in the different media.

Test for $TbFeO_3$ powder	pH	m_{final} (g)	L^*	a^*	b^*	ΔE^*
Air	–	0.2500	60.47	21.94	32.22	–
Acid	0.27	0.2445	60.27	21.54	32.29	0.45
Alkali	13.52	0.2454	60.33	21.48	31.97	0.54
Water	6.28	0.2476	60.80	21.83	32.54	0.47

As a result, reddish cool pigments without any toxic elements were developed in the present work for application in a siloxane paint and two different frits. Specifically, $GdFeO_3$, $TbFeO_3$ and

$YFeO_3$ samples, which have the reddest colouration with frit A, presented the highest NIR solar reflectance values, making them good cool pigments.

4. Conclusions

High NIR reflectance reddish pigments with the general formula $AFeO_3$ (A = La, Pr, Nd, Sm, Gd, Tb, Y or Yb) were synthesised by a coprecipitation method. The orthorhombic perovskite with the *Pbnm* space group was observed in all samples without any secondary phase. Absorption and reflectance measurements in the UV–Vis range confirmed that these pigments present a reddish colour with a band gap range between 1.94 and 2.13 eV. Furthermore, good stability of pigments in a siloxane paint and two glazes was obtained. On comparing the coatings of all the coloured paints, it is found that mixes containing $GdFeO_3$, $TbFeO_3$ and $YFeO_3$ powders possess the highest NIR solar reflectance, reaching values of R = 50%. They could therefore be considered good cool pigments. The variation in the indoor temperature after application of two coats of paint, one with commercial reddish pigment and the other with $TbFeO_3$ powder, reaches 3.2 °C, the lowest temperature being achieved by the building with the coating of the $TbFeO_3$ powder–paint mixture. The CIE$L^*a^*b^*$ and CIE$L^*C^*H^*$ parameters also indicate that the mixtures of frit A with the three pigments mentioned above also present the reddest tone. Moreover, $TbFeO_3$ powder, which presents the highest NIR solar reflectance, is also thermally and chemically stable. As a result, the synthesised compounds are good candidates for use as reddish pigment in glazes for ceramic tiles and also as cool roofing materials.

Declaration of competing interest

The authors declare that they have no known competing financial interests or personal relationships that could have appeared to influence the work reported in this paper.

Acknowledgements

Authors thanks the Universitat Jaume I [UJI-B2019-41] and the Ministerio de Economía, Industria y Competitividad [MAT2016-80410-P] for financial support. P. Serna also thanks the Ministerio de Ciencia, Innovación y Universidades for an FPU predoctoral contract.

Appendix A. Supplementary data

Supplementary data to this article can be found online at https://doi.org/10.1016/j.jmat.2021.02.002.

References

[1] Ma X, Guo Y, Shi G, Yu Y. Numerical simulation of global temperature change during the 20th century with the IAP/LASG GOALS model. Adv Atmos Sci 2004;21:227–35. https://doi.org/10.1007/BF02915709.
[2] Pörtner HO. Climate change and temperature-dependent biogeography: oxygen limitation of thermal tolerance in animals. Naturwissenschaften 2001;88:137–46. https://doi.org/10.1007/s001140100216.
[3] Lim YK, Cai M, Kalnay E, Zhou L. Impact of vegetation types on surface temperature change. J Appl Meteorol Climatol 2008;47:411–24. https://doi.org/10.1175/2007JAMC1494.1.
[4] Wang X, Piao S, Ciais P, Li J, Friedlingstein P, Koven C, et al. Spring temperature change and its implication in the change of vegetation growth in North America from 1982 to 2006. Proc Natl Acad Sci U S A 2011;108:1240–5. https://doi.org/10.1073/pnas.1014425108.
[5] Skripnuk DF, Samylovskaya EA. Human activity and the global temperature of the planet. IOP Conf Ser Earth Environ Sci 2018;180:012021. https://doi.org/10.1088/1755-1315/180/1/012021.
[6] Philipona R, Dürr B, Ohmura A, Ruckstuhl C. Anthropogenic greenhouse forcing and strong water vapor feedback increase temperature in Europe. Geophys Res Lett 2005;32:L19809. https://doi.org/10.1029/2005GL023624.
[7] Synnefa A, Santamouris M, Apostolakis K. On the development, optical properties and thermal performance of cool colored coatings for the urban environment. Sol Energy 2007;81:488–97. https://doi.org/10.1016/j.solener.2006.08.005.
[8] Thejus PK, Krishnapriya KV, Nishanth KG. A cost-effective intense blue colour inorganic pigment for multifunctional cool roof and anticorrosive coatings. Sol Energy Mater Sol Cells 2021;219:110778. https://doi.org/10.1016/j.solmat.2020.110778.
[9] Baneshi M, Maruyama S, Komiya A. The effects of using some common white pigments on thermal and aesthetic performances of pigmented coatings. J Therm Sci Technol 2009;4:131–45. https://doi.org/10.1299/jtst.4.131.
[10] Jose S, Joshy D, Narendranath SB, Periyat P. Recent advances in infrared reflective inorganic pigments. Sol Energy Mater Sol Cells 2019;194:7–27. https://doi.org/10.1016/j.solmat.2019.01.037.
[11] Cerro S, Llusar M, Gargori C, Monrós G. Cool and photocatalytic yellow ceramic pigments; from lead-tin to Cr doped scheelite pigments. Ceram Int 2019;45:4613–25. https://doi.org/10.1016/j.ceramint.2018.11.150.
[12] Huang B, Xiao Y, Huang C, Chen J, Sun X. Environment-friendly pigments based on praseodymium and terbium doped $La_2Ce_2O_7$ with high near-infrared reflectance: synthesis and characterization. Dyes Pigments 2017;147:225–33. https://doi.org/10.1016/j.dyepig.2017.08.004.
[13] Dolić SD, Jovanović DJ, Štrbac D, Far LĐ, Dramićanin MD. Improved coloristic properties and high NIR reflectance of environment-friendly yellow pigments based on bismuth vanadate. Ceram Int 2018;44:22731–7. https://doi.org/10.1016/j.ceramint.2018.09.057.
[14] Orna MV. Chemistry, color, and art. J Chem Educ 2001;78:1305. https://doi.org/10.1021/ed078p1305.
[15] Jovaní M, Sanz A, Beltrán-Mir H, Cordoncillo E. New red-shade environmental-friendly multifunctional pigment based on Tb and Fe doped $Y_2Zr_2O_7$ for ceramic applications and cool roof coatings. Dyes Pigments 2016;133:33–40. https://doi.org/10.1016/j.dyepig.2016.05.042.
[16] Jovaní M, Fortuño-Morte M, Beltrán-Mir H, Cordoncillo E. Environmental-friendly red-orange ceramic pigment based on Pr and Fe co-doped $Y_2Zr_2O_7$. J Eur Ceram Soc 2018;38:2210–7. https://doi.org/10.1016/j.jeurceramsoc.2017.12.005.
[17] Fortuño-Morte M, Beltrán-Mir H, Cordoncillo E. Study of the role of praseodymium and iron in an environment-friendly reddish orange pigment based on Fe doped $Pr_2Zr_2O_7$: a multifunctional material. J Alloys Compd 2020;845:155841. https://doi.org/10.1016/j.jallcom.2020.155841.
[18] Pyon K-R, Lee B-H. Effect of iron content and annealing temperature on the color characteristics of Fe-$ZrSiO_4$ coral pink pigments synthesized by sol-gel method. J Ceram Soc Japan 2009;117:258–63. https://doi.org/10.2109/jcersj2.117.258.
[19] Chu HL, Wang CL, Hwang WS, Lee KC, Zhou X, Wang MC. Kinetics of phase transformation and optical property of pink coral zirconia powders. J Alloys Compd 2014;601:307–18. https://doi.org/10.1016/j.jallcom.2014.02.136.
[20] Zumaquero E, Orts MJ, Sanz V, Mestre S. Iron zircon pigment synthesis: proposal of a mixing index for the raw materials mixtures. Bol Soc Esp Ceram V 2017;56:177–85. https://doi.org/10.1016/j.bsecv.2017.01.003.
[21] Cappelletti G, Ardizzone S, Fermo P, Gilardoni S. The influence of iron content on the promotion of the zircon structure and the optical properties of pink coral pigments. J Eur Ceram Soc 2005;25:911–7. https://doi.org/10.1016/j.jeurceramsoc.2004.04.023.
[22] Herrera G, Montoya N, Alarcón J. Synthesis and characterization of iron-doped $ZrSiO_4$ solid solutions from gels. J Am Ceram Soc 2011;94:4247–55. https://doi.org/10.1111/j.1551-2916.2011.04808.x.
[23] Herrera-Pérez GM. Iron doped-$ZrSiO_4$: structural, microstructural and vibrational characterization. Mater Res 2015;18:1313–21. https://doi.org/10.1590/1516-1439.025215.
[24] Raj AKV, Rao PP, Sameera S, Divya S. Pigments based on terbium-doped yttrium cerate with high NIR reflectance for cool roof and surface coating applications. Dyes Pigments 2015;122:116–25. https://doi.org/10.1016/j.dyepig.2015.06.021.
[25] Raj AKV, Rao PP, Sreena TS, Thara TRA. Pigmentary colors from yellow to red in $Bi_2Ce_2O_7$ by rare earth ion substitutions as possible high NIR reflecting pigments. Dyes Pigments 2019;160:177–87. https://doi.org/10.1016/j.dyepig.2018.08.010.
[26] George G, Vishnu VS, Reddy MLP. The synthesis, characterization and optical properties of silicon and praseodymium doped Y_6MoO_{12} compounds: environmentally benign inorganic pigments with high NIR reflectance. Dyes Pigments 2011;88:109–15. https://doi.org/10.1016/j.dyepig.2010.05.010.
[27] Sarasamma Vishnu V, Lakshmipathi Reddy M. Near-infrared reflecting inorganic pigments based on molybdenum and praseodymium doped yttrium cerate: synthesis, characterization and optical properties. Sol Energy Mater Sol Cells 2011;95:2685–92. https://doi.org/10.1016/j.solmat.2011.05.042.
[28] Liu L, Han A, Ye M, Zhao M. Synthesis and characterization of Al^{3+} doped $LaFeO_3$ compounds: a novel inorganic pigments with high near-infrared reflectance. Sol Energy Mater Sol Cells 2015;132:377–84. https://doi.org/10.1016/j.solmat.2014.08.048.
[29] Hosokawa S, Matsumoto S, Onishi K, Asakura H, Teramura K, Tanaka T. CO and C_3H_6 oxidation over platinum-group metal (PGM) catalysts supported on Mn-modified hexagonal $YbFeO_3$. Catal Today 2019;332:183–8. https://doi.org/10.1016/j.cattod.2018.07.026.
[30] Chen Y, Wang D, Qin H, Zhang H, Zhang Z, Zhou G, et al. CO_2 sensing

properties and mechanism of $PrFeO_3$ and $NdFeO_3$ thick film sensor. J Rare Earths 2019;37:80–7. https://doi.org/10.1016/j.jre.2018.06.007.
[31] Luxová J, Šulcová P. The effect of partial substitution of Bi on colour properties and thermal stability of $Bi_xPr_{1-x}FeO_3$ pigments. J Therm Anal Calorim 2019;138:4303–12. https://doi.org/10.1007/s10973-019-08686-8.
[32] Cunha JD, Melo DMA, Martinelli AE, Melo MAF, Maia I, Cunha SD. Ceramic pigment obtained by polymeric precursors. Dyes Pigments 2005;65:11–4. https://doi.org/10.1016/j.dyepig.2004.06.005.
[33] Dohnalová Z, Sulcová P, Trojan M. Synthesis and characterization of $LnFeO_3$ pigments. J Therm Anal Calorim 2008;91:559–63. https://doi.org/10.1007/s10973-007-8636-0.
[34] Piña PC, Buentello R, Arriola H, Nava EN. Mössbauer spectroscopy of lanthanum and holmium ferrites. Hyperfine Interact 2008;185:173–7. https://doi.org/10.1007/s10751-008-9823-5.
[35] Piña C, Arriola H, Nava N. Mössbauer study of iron perovskites of Er, Sm and Nd. J Phys Conf Ser 2010;217:012036. https://doi.org/10.1088/1742-6596/217/1/012036.
[36] Luxová J, Šulcová P, Trojan M. Influence of firing temperature on the color properties of orthoferrite $PrFeO_3$. Thermochim Acta 2014;579:80–5. https://doi.org/10.1016/j.tca.2014.01.017.
[37] Opuchovic O, Kreiza G, Senvaitiene J, Kazlauskas K, Beganskiene A, Kareiva A. Sol-gel synthesis, characterization and application of selected sub-microsized lanthanide (Ce, Pr, Nd, Tb) ferrites. Dyes Pigments 2015;118:176–82. https://doi.org/10.1016/j.dyepig.2015.03.017.
[38] Burkovičová A, Dohnalová Ž, Šulcová P. Preparation and evaluation of the color properties of $YFeO_3$ pigments doped by In^{3+} and Ga^{3+}. Ceram - Silikaty 2017;61:34–9. https://doi.org/10.13168/cs.2016.0057.
[39] Yuan L, Han A, Ye M, Chen X, Yao L, Ding C. Synthesis and characterization of environmentally benign inorganic pigments with high NIR reflectance: lanthanum-doped $BiFeO_3$. Dyes Pigments 2018;148:137–46. https://doi.org/10.1016/j.dyepig.2017.09.008.
[40] Rodriguez-Carvajal J, Fullprof Program. Phys B 1993;192:55–69.
[41] Astm G. 173–03: standard tables for reference solar spectral irradiances: direct normal and hemispherical on 37 tilted surface. West Conshohocken, PA: ASTM International; 2003.
[42] Weber MC, Guennou M, Zhao HJ, Íñiguez J, Vilarinho R, Almeida A, et al. Raman spectroscopy of rare-earth orthoferrites $RFeO_3$ (R =La, Sm, Eu, Gd, Tb, Dy). Phys Rev B 2016;94:214103. https://doi.org/10.1103/PhysRevB.94.214103.
[43] Hepting M. Ordering phenomena in rare-earth nickelate heterostructures. Springer Theses; 2017.
[44] Saha J, Jana YM, Mukherjee GD, Mondal R, Kumar S, Gupta HC. Structure, Mössbauer spectroscopy and vibration phonon spectra in valence-bond force-field model approach for distorted perovskites $AFeO_3$ (A = La, Y). Mater Chem Phys 2020;240:122286. https://doi.org/10.1016/j.matchemphys.2019.122286.
[45] Jia YQ. Crystal radii and effective ionic radii of the rare earth ions. J Solid State Chem 1991;95:184–7. https://doi.org/10.1016/0022-4596(91)90388-X.
[46] Zaza F, Pallozzi V, Serra E, Pasquali M. Combustion synthesis of $LaFeO_3$ sensing nanomaterial. AIP Conf Proc 2015:1–11. https://doi.org/10.1063/1.4922559.020003.
[47] Wang W, Sun W, Zhang G, Cheng Z, Wang Y. Magnetic domain-wall induced ferroelectric polarization in rare-earth orthoferrites $AFeO_3$ (A = Lu, Y, Gd): first-principles calculations. J Mater Chem C 2019;7:10059–65. https://doi.org/10.1039/c9tc02501d.
[48] Gupta S, Medwal R, Pavunny SP, Sanchez D, Katiyar RS. Temperature dependent Raman scattering and electronic transitions in rare earth $SmFeO_3$. Ceram Int 2018;44:4198–203. https://doi.org/10.1016/j.ceramint.2017.11.223.
[49] Ahmad Mir F, Ikram M, Kumar R. Temperature-dependent Raman study of $PrFeO_3$ thin film. J Raman Spectrosc 2011;42:201–8. https://doi.org/10.1002/jrs.2655.
[50] Singh MK, Jang HM, Gupta HC, Katiyar RS. Polarized Raman scattering and lattice eigenmodes of antiferromagnetic $NdFeO_3$. J Raman Spectrosc 2008;39:842–8. https://doi.org/10.1002/jrs.1923.
[51] Matteucci F, Cruciani G, Dondi M, Gasparotto G, Tobaldi DM. Crystal structure, optical properties and colouring performance of karrooite $MgTi_2O_5$ ceramic pigments. J Solid State Chem 2007;180:3196–210. https://doi.org/10.1016/j.jssc.2007.08.029.
[52] Binnemans K, Görller-Walrand C. On the color of the trivalent lanthanide ions. Chem Phys Lett 1995;235:163–74. https://doi.org/10.1016/0009-2614(95)00126-O.
[53] O'Donoghue M. Gemstones. Chapman and Hall; 1988.

María Fortuño-Morte: Maria Fortuño-Morte received her Chemistry Degree and the University Master's Degree in Applied and Pharmacological Chemistry from University Jaume I, Spain, in 2015 and 2016, respectively. She is currently carrying out her Ph.D. research at the same university. Her research focuses on environment-friendly inorganic pigments with multifunctional applications.

Pablo Serna-Gallén: Pablo Serna-Gallén is graduated in Chemistry with honors from the University Jaume I, Spain, and got a Master's Degree in Applied and Pharmacological Chemistry with further specialization in Advanced Materials. Currently developing his Ph.D. degree at the same university, his research focuses on optical materials with fluoride-type structures. He has obtained numerous important national and local awards for his academic marks and research.

Héctor Beltrán Mir: Dr. Héctor Beltrán-Mir is currently an Associate Professor of Inorganic Chemistry at the University Jaume I of Castellón, Spain, and researcher of the Solid State Group since 1997. He received his Ph.D. degree in Chemistry in 2001. He spent two years (2002–2003) as a postdoctoral researcher at the Department of Material Science and Engineering at the University of Sheffield (UK) under the supervision of Professor Anthony R. West. His current research interest is mainly focused on the synthesis and characterization of Inorganic Materials, especially oxides, with interesting and/or useful optical and electrical properties. The materials studied cover the fields of: 1) electroceramic materials, characterized mainly by impedance spectroscopy; 2) inorganic pigments for multifunctional applications, and 3) nanomaterials, generated by the irradiation of different oxides using femtosecond laser. He is author and/or co-author of over 60 papers in international peer-reviewed journals of high impact, a book chapter and a patent.

Eloísa Cordoncillo: Prof. Eloisa Cordoncillo, has more than 30 years' experience in applied materials research. She received her PhD in 1995 in Inorganic Chemistry, at Jaume I University of Castellón. She is Full Professor of Inorganic Chemistry and researcher of the Solid State Chemistry group. Her interests include the synthesis, characterization and application of ceramic pigments with low environmental impact by using lanthanide ions and soft chemistry routes to prepare materials with interesting optical and electrical properties. She is the co-author of over 120 high-impact scientific publications, book chapters and proceedings.